Polarization patterns in refracting structures

Barbara K. Pierscionek

School of Electronic Engineering, La Trobe University Bundoora, Victoria 3083, Australia

John Lekner

Department of Physics, Victoria University of Wellington, Wellington, New Zealand

Received March 27, 1996; revised manuscript received September 23, 1996; accepted September 23, 1996

The effect of refraction on linearly polarized light was investigated by photographing two refracting bodies placed between linear polarizers that were lying in parallel planes, for varying angles between the transmission axes of the polarizers. The light intensity distributions from representative quadrants in the positive images were measured and compared with theoretical predictions for the crossed and the parallel polarizer conditions. © 1997 Optical Society of America [S0740-3232(97)00603-0]

Key words: isogyres, light intensity patterns, refraction, polarization.

1. INTRODUCTION

The formation of isogyres, characteristic dark cross patterns seen in refracting structures placed between crossed linear polarizers, has recently been qualitatively understood[1] and compared with theory.[2–4] The cross pattern is formed because, as the light passes through the structure, there is a rotation of the plane-polarized light in all planes except those parallel to the polarizer and analyzer axes, and the extent of this rotation varies depending on the path that the light takes. Consequently, some light is able to pass through the second polarizer (analyzer), and there are variations in the light intensity within the quadrants that separate the isogyres.

Isogyres can form between crossed polarizers if a change in the direction of the electric vector produces a component parallel to the analyzer axis. Hence they are seen in birefringent crystals placed between crossed polarizers in convergent light and can even be formed with large angular apertures and by rays obliquely incident on a polarizer without any refracting structure in place.[5] In the latter case it has been shown that the ray polarization direction and hence the proportion of light transmitted through the analyzer can be calculated from the angle of incidence of the oblique rays.

This paper aims to investigate the polarization patterns seen in refracting structures placed between two polarizers that are lying in parallel planes, for varying angles between the polarizer transmission axes. Light intensity distributions, measured along a line that bisects a quadrant of each of the resultant images, are compared with theoretical predictions for the crossed and the parallel polarizers.

2. METHODS

Two refracting structures were used: a perspex spheroid of refractive index 1.492 and diameters 10.5 mm (major) and 9.0 mm (minor), and a spherical vitamin *E* pill with refractive index of 0.4-mm-thick gelatin shell 1.482, refractive index of oil within 1.511, and diameter 7 mm, labeled S1 and S2, respectively. Each was placed on a sheet of linear polarizer (Lee camera filter; extinction, as measured with a Hagener S2 photometer for the light source used in these experiments, was 3.9×10^{-4}) on top of a diffuse source: a light box (Leitz, Type 42-677.103; 3200 K color temperature). Above the structure, supported on a stand 38 mm in height, rested the analyzer, the edges of which were attached to a ring with angular demarcations, allowing quantifiable rotation in a plane parallel to the plane of the polarizer. A camera (Nikon F4S camera with a 105-mm Micro Nikkor lens) was placed in position 35 cm above the light box and was focused on the test structure. Kodak EPY 64T film (producing positive images) was used. The height of the camera above the object was sufficient for the image rays to be effectively parallel.

Photographs were taken for angles of 0°, 30°, 45°, 60°, and 90° between the analyzer and polarizer axes. All photographs were taken with *f*/#22 and exposures of 16, 20, and 24 s when the polarizer axes were 90° apart and 4, 8, and 12 s for all other angles. The longer exposure times for the crossed polarizer images were because of the lowered light levels. Exposures at 16 s for the crossed polarizer images and at 4 s for all the other images were selected for analysis. The shorter exposure times were selected to avoid saturated values in the scanning procedure.

The amount of light transmitted through the two polarizers, for varying angles χ between polarizer transmission axes, was measured with a Hagener S2 photometer for angles of 0°, 15°, 30°, 45°, 60°, and 90°. This served to determine whether the light transmission through the two polarizers followed the law described by Malus, which describes the amount of light that passes through two polarizers lying in parallel planes as

$$I = I_0 \cos^2 \chi,$$

where I_0 is the incident light intensity and I is the light transmitted for varying angles χ.

0740-3232/97/030676-06$10.00

Positives were scanned with a Nikon Coolscan (Nikon 35-mm scanner LS-10E standard model). The scanned images were loaded onto an IBM-compatible (486, 33 MHz) computer with a super VGA monitor and displayed with the aid of a Matrox IP-A frame grabber. A representative quadrant for each structure was selected. A *C* program, which read relative light intensity (RI) values from an x, y coordinate system fitted to the quadrant, determined RI values along the line $x = y$ (i.e., along the radial bisector of the quadrant). Units of RI were graded from 0 to 255. All values were below or equal to 254 (i.e., there was no saturation).

All RI values and positions along the radius $x = y$ were normalized. RI values at 0.2, 0.4, 0.6, and 0.8 of the radial distance from the center, as well as values outside the quadrant, were selected for analysis. We used these latter surround RI values as controls of the photometric measurements to see whether there was any distortion or nonlinearity of the light transmittance by the scanning and densitometric procedures (i.e., to check the appropriateness of the gamma curve used by the instrument). We had also checked the gamma curve previously by photographing six calibrated neutral-density filters (Ealing 26-5868 ND filter set) and subjecting the images of the filters to the same analysis procedure as the test images.[6] Calculated density values (determined from light transmittance measured with the image scanner) were very close to the nominal neutral-density values, and the relationship between the two sets was indeed linear. Graphical analysis of data was done with Cricket graph (1.3.2) on a Macintosh PowerBook 140 computer.

3. RESULTS

A. Experimental Observations

Figure 1 shows the images formed by S1 and S2 with alteration of the angles between the polarizers from 90° (crossed) to 0° (parallel). In both, the outer parts of the cross arms rotate while the central sections become gradually lighter and lose definition as the angle between the polarizer axes decreases. In the parallel position (0° between polarizers), there is a diffuse, light cross with darker sections in the four quadrants, i.e., a reversal of the pattern seen between crossed polarizers. (The contrast of the crossed polarizer figures has been enhanced by the printing process, and so the quadrants appear considerably lighter in these photographs than indicated by the measurements.)

Photometric measurements of light transmittance through the two polarizers alone for varying χ showed a linear relationship ($p \ll 0.01$) against $\cos^2 \chi$ (Table 1) in accordance with the law of Malus. Surround intensity values (i.e., light transmittance through the two polarizers only) taken from the negatives also produced statistically significant ($p < 0.05$) linear relations against $\cos^2 \chi$ (Table 1), confirming that there was no distortion in the scanning procedure. (The surround values from the crossed polarizer images were not included in these linear relationships, because these images had been taken at an exposure different from that for the other images.)

We analyzed each of the images from both structures by scanning a representative quadrant in each image and

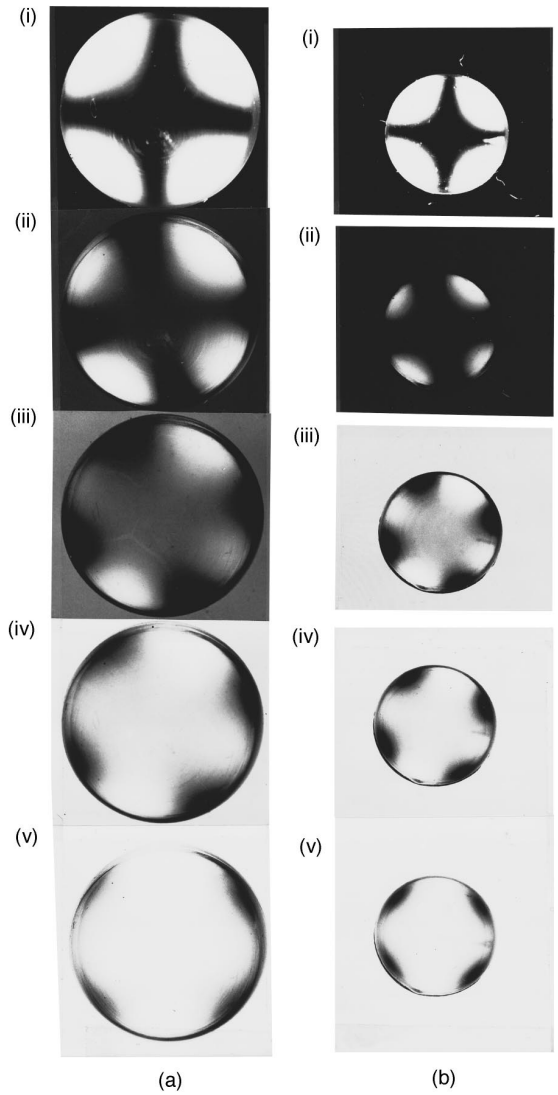

Fig. 1. Images seen in (a) S1 and (b) S2 illuminated by diffuse light and photographed between linear polarizers. The angles between the polarizers (χ) are altered in a stepwise fashion: (i) 90° (crossed polarizers), (ii) 60°, (iii) 45°, (iv) 30°, and (v) 0° (parallel polarizers).

Table 1. Functions Describing Relationships between Light Intensity Values (RI) and Angles (χ)[a]

Refracting Structure	K1	K2	r^2	p
Light transmission measured with a Hagener photometer				
	6.119	312.62	0.998	<0.01
RI of surround measured by densitometric scanning of positives				
S1	0.1498	0.8911	0.960	<0.05
S2	0.1703	0.8563	0.983	<0.01

[a] $RI = K1 + K2 \cos^2 \chi$, where the angle χ is between transmission axes of the polarizers, K1, K2 are constants, r^2 is the correlation coefficient, and p is the significance level.

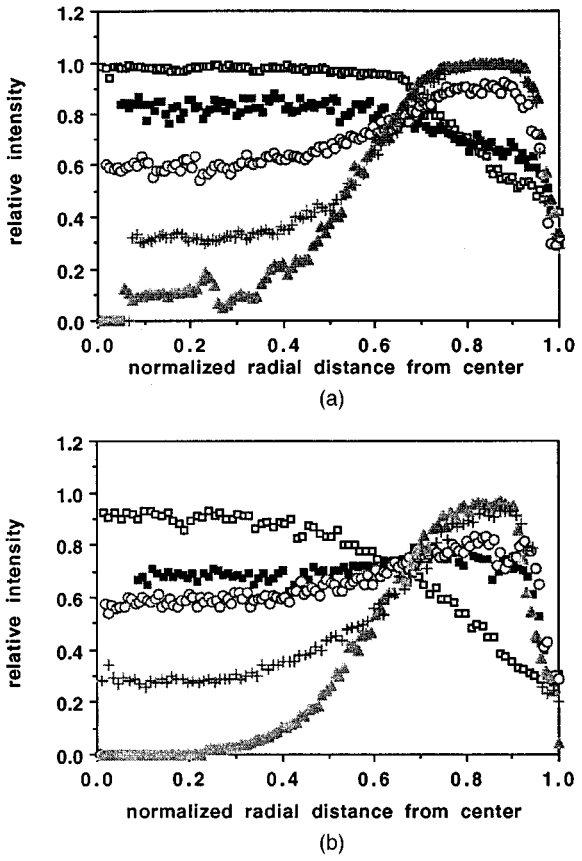

Fig. 2. Relative light intensity (RI) distributions in representative quadrants determined by scanning photographic positives from (a) S1 and (b) S2, plotted against the normalized radial distance from the center (D). Open squares, $\chi = 0°$; filled squares, $\chi = 30°$; circles, $\chi = 45°$; crosses, $\chi = 60°$; triangles, $\chi = 90°$.

measuring the RI distribution along the line that diagonally bisects the quadrant ($x = y$). The RI values are shown in Figs. 2(a) and 2(b) plotted against the normalized radial distance from the center (D). For both structures the values decrease in the center and increase in the periphery of the quadrant as χ increases. In Fig. 2(a) the decrease in RI in the central regions occurs in fairly even steps. Between $D = 0.6$ and $D = 0.7$ the RI values in all images are similar, at ~0.8–0.9 of the maximum RI. For S2 [Fig. 2(b)] the functions again meet at ~$D = 0.6$–0.7, where the RI is ~0.7–0.8. Unlike in Fig. 2(a), the decreases in intensity in the central regions here are nonlinear. (N.B.: The crossed polarizer images were taken with a longer exposure time, and hence the intensity values appear to be in the same range as for the other images.)

B. Theoretical Analysis

The existing theory[1–3] does not take into account two experimental realities, namely, that the illumination is not ideally diffuse and that the polarizer transmittance depends on the angle of incidence. Both of these factors are important in the isogyre patterns.

Figure 3 (adapted from Ref. 3) shows the path of a ray through the refracting body. When the exiting ray is paraxial (as we assume here), the angle that the incident ray makes with the x axis is $\Psi = \theta_1 - \theta_2 + \theta_1' - \theta_2'$. For a sphere this simplifies to $\Psi = 2(\theta_1 - \theta_2)$. The largest possible value of θ_1 is 90° (at glancing incidence), and the largest Ψ for a sphere is thus 180° $- 2\arcsin(n_1/n_2)$. This exceeds 90° when $n_2/n_1 > \sqrt{2}$, and thus for spheres of relative refractive index greater than $\sqrt{2}$ some of the outer rays will not be pro-

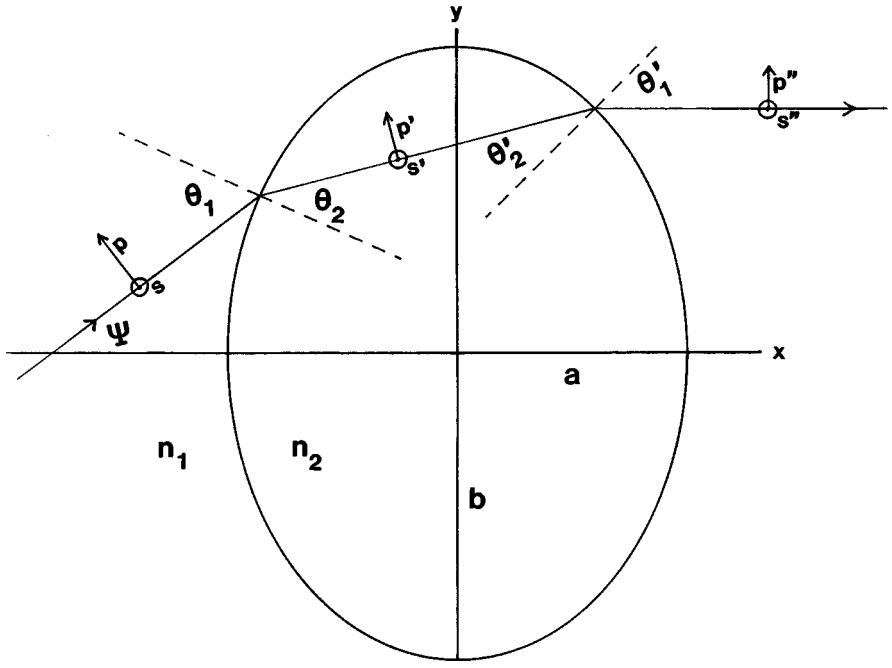

Fig. 3. Ray path through a homogeneous and isotropic lens. The ray crosses the axis at angle Ψ, and its angle of incidence is θ_1. The lens has refractive index n_2 and lies in a medium of index n_1. The light is a mixture of p and s polarizations (p has electric vector in the plane of the figure; s has electric vector normal to the figure).

duced by illumination from a half-plane. For an ideal Lambertian surface (approximated by our light box) the distribution of illumination is given by $I(\Psi) = I(0)\cos\Psi$ ($\Psi \leqslant 90°$).

The transmission through the polaroid differs from the ideal given in Eqs. (1) of Ref. 3, namely, from $E_p = E_0 \cos\phi$ and $E_s = E_0 \sin\phi$, where E_p and E_s are the transmitted electric field amplitudes in the p- and s-polarization directions and ϕ is the angle between the transmission axis of the polarizer and the plane of Fig. 3. To calculate the transmission through the polaroid filter, we will model it as a uniaxial absorbing layer with optic axis in the plane of the polaroid (the transmission axis is also in the plane of the polaroid and is perpendicular to the optic axis). An actual polaroid is a layered structure: for example, the HN22 consists of two polyvinyl-alcohol-iodine H-type polarizer layers, 16–20 μm thick, laminated in the direction parallel to opposite sides of a 100-μm-thick sheet of cellulose acetate butyrate; the assembly is laminated between protective covers of plastic or glass. The real parts of the refractive indices (n_o and n_e for the polarizer layers) will be assumed to be nearly equal to the refractive index n of the cellulose acetate butyrate (1.475 at the sodium-D line) and to that of the protective covers. Because of the absorption within the polarizer layers, we can neglect multiple reflections within the structure. With these approximations, the theory of the optical properties of a uniaxial layer (developed for normal and general incidence[7,8]) gives the transmission amplitudes

$$t_{pp} \approx t\frac{k_1^2k^4\cos^2\phi}{(k^2q_1 + k_1^2q)^2},$$

$$t_{ps} = t_{sp} \approx -t\frac{k_1qk^2\cos\phi\sin\phi}{(k^2q_1 + k_1^2q)(q_1 + q)},$$

$$t_{ss} \approx t\frac{q^2\sin^2\phi}{(q_1 + q)^2},$$

where $k_1 = n_1\omega/c$, $k = n\omega/c$, $q_1 = k_1\cos\Psi$, $q = k\cos\theta$, and θ is found from $n_1\sin\Psi = n\sin\theta$; note that Ψ is the angle of incidence for the polaroid. The common transmission factor t is given by

$$t = \frac{4q_1q\exp(-q_i\Delta z)}{q^2\sin^2\phi + k^2\cos^2\phi}.$$

Here Δz is the thickness of the absorbing part of the polaroid laminate and q_i is the (small) imaginary part of the normal component of the ordinary wave vector in the polarizer layers.

These transmission amplitudes give the fields transmitted for a particular linear polarization of the incident light. For example, t_{ps} gives the s-polarized transmitted amplitude when unit amplitude p-polarized light is incident. We need to calculate the transmission for unpolarized light, and to do this we will average over light linearly polarized in random directions. If a given wave of unit amplitude is linearly polarized at angle ξ to the p direction, the electric fields transmitted along the s and p directions will be

$$E_p = t_{pp}\cos\xi + t_{sp}\sin\xi,$$

$$E_s = t_{ps}\cos\xi + t_{ss}\sin\xi.$$

The averages of $|E_p|^2$ and $|E_s|^2$ over all angles ξ are

$$\langle|E_p|^2\rangle = 1/2(|t_{pp}|^2 + |t_{sp}|^2),$$

$$\langle|E_s|^2\rangle = 1/2(|t_{ss}|^2 + |t_{ps}|^2).$$

Thus the transmission amplitudes along the p and s directions for unpolarized light are

$$\tau_p = [(|t_{pp}|^2 + |t_{sp}|^2)/2]^{1/2},$$

$$\tau_s = [(|t_{ss}|^2 + |t_{ps}|^2)/2]^{1/2}.$$

From our approximate formulas for t_{ss}, $t_{ps} = t_{sp}$, and t_{ss}, we find that

$$\tau_p \approx \frac{tQ^4}{\sqrt{2}(k^2q_1 + k_1^2q)(q_1 + q)}\frac{k_1k^2\cos\phi}{k^2q_1 + k_1^2q} \equiv f_p\cos\phi,$$

$$\tau_s \approx \frac{tQ^4}{\sqrt{2}(k^2q_1 + k_1^2q)(q_1 + q)}\frac{q\sin\phi}{q_1 + q} \equiv f_s\sin\phi,$$

where

$$Q^8 = k_1^2k^4(q_1 + q)^2\cos^2\phi + q^2(k^2q_1 + k_1^2q)^2\sin^2\phi.$$

The factors τ_p and τ_s replace the ideal polarizer values $\cos\phi$ and $\sin\phi$ used by Lekner.[3] The main dependence on ϕ (the angle between the transmission axis of the polarizer and the plane of Fig. 3) remains in the $\cos\phi$ and $\sin\phi$ factors, since the ϕ dependence of tQ^4 is weak. At normal incidence the factors f_p and f_s are equal, and at glancing incidence they both go to zero, in the ratio $f_p/f_s \to n^2/n_1(n^2 - n_1^2)^{1/2}$. This ratio has the minimum value of 2 (when $n = \sqrt{2}n_1$); thus there are substantial and different corrections to the $\cos\phi$, $\sin\phi$ factors for large angles of incidence.

The net result of these considerations is to replace Eq. (7) of Ref. 3 for the electric field along the transmission axis of the analyzer (at angle χ to the polarizer transmission axis) with

$$E_a = \sqrt{I(\Psi)}[t_pt_p'f_p\cos\phi\cos(\phi + \chi) + t_st_s'f_s\sin\phi\sin(\phi + \chi)].$$

[We have assumed that light passes normally through the analyzer and have omitted the attenuation factor for the analyzer. The transmission amplitudes t_p, t_s and t_p', t_s' are for the object under study and are defined in Eqs. (4) and (5) of Ref. 3]. The transmitted intensity is proportional to the square of E_a. To plot this, we need to know the angular dependence of the transmission factor $T(\Psi) = \exp(-2q_i\Delta z)$. We have $q_i \approx k_in/(n^2 - n_1^2\sin^2\Psi)^{1/2}$ [see Eq. (8.12) of Ref. 9], and thus

$$T(\Psi) \approx [T(0)]^{n/(n^2 - n_1^2\sin^2\Psi)^{1/2}}$$

The transmission factor decreases with increasing angle of incidence onto the polarizer.

Variations in the squares of the transmission factors f_s and f_p with the angle of incidence on the polarizer are shown in Fig. 4 for $\phi = 45°$. The effects of correcting for these variations and for the Lambertian illumination are shown in Fig. 5, in which relative intensities for a struc-

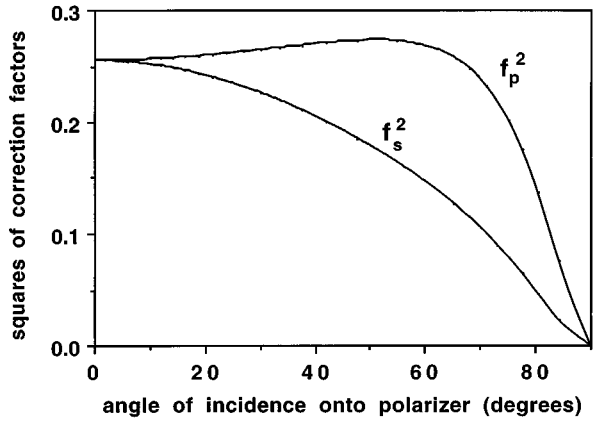

Fig. 4. Squares of the transmission factors f_s and f_p plotted against angle of incidence on the polarizer for $\phi = 45°$.

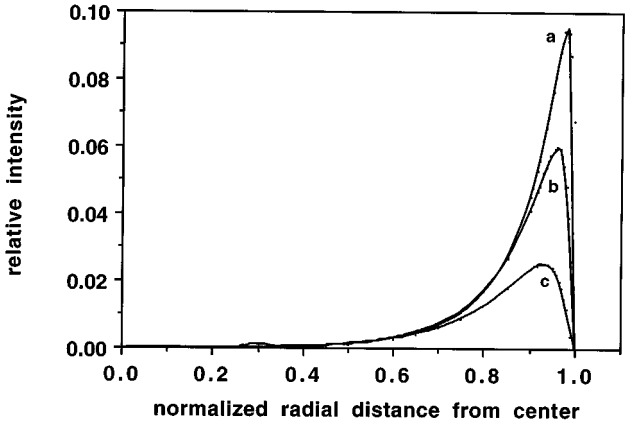

Fig. 5. Relative intensity plotted against angle of incidence on the polarizer for a value of $\phi = 45°$: curve a, for an ideal polarizer; curve b, with transmission factors f_s and f_p included; curve c, with transmission factors and Lambertian illumination (with cos Ψ factor).

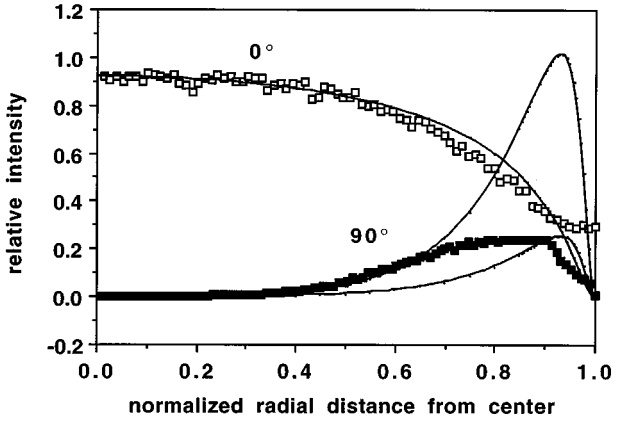

Fig. 6. Comparison of theoretical and experimental variations (for S2) for crossed ($\chi = 90°$) and parallel ($\chi = 0°$) polarizers showing relative light intensity plotted against normalized radial distance from the center. The theoretical curves are shown as line graphs, and the experimental data are denoted by symbols. Note that the fourfold increase in exposure time for the crossed polarizer image has been accounted for. The theoretical curves for $\chi = 90°$ intensity have been multiplied by 10 and 40 to fit the experimental data in terms of peak height and for the rising part of the curve, respectively.

ture modeled on S2 between crossed polarizers and for $\phi = 45°$ are plotted against the normalized radial distance from the center. With corrections, from the ideal polarizer model to the model that incorporates both transmission factors and corrects for Lambertian illumination, the peak value drops substantially and the peak shifts away from the edge of the structure. The full theory is used in the calculations of intensity distributions for the HN22 polarizer in air ($n_1 = 1$) with $T(0) = 0.55$, $n = 1.475$. These theoretical curves are compared with experimental data for S2 in Fig. 6 for intensities at $\chi = 0°$ and 90°. $I(\Psi) = I(0)\cos\Psi$ for $\Psi \leqslant 90°$ has been assumed, and the experimental data for the crossed polarizers have been divided by 4 to compensate for the fourfold increase in exposure time used in photography of these images. (The reciprocity relation for the film is valid over the exposure range in this work. Hence the intensities of the images taken with longer exposures can be divided by the ratio of exposure times, i.e., 16:4.) The theoretical curve for crossed polarizers has been multiplied by 10 to facilitate comparison.

4. DISCUSSION

We have measured the intensity distributions in the polarization patterns seen in two refracting structures when the angle between the transmission axes of the polarizers is varied. In the inner regions of both structures, most light emerged when the polarizer axes were parallel, which indicated very little alteration to the initial polarization state of the light. This finding is consistent with the finding that the inner regions appeared dark between crossed polarizers. Conversely, close to the edge, the maximum RI occurs when the polarizers are crossed, and there are dark spots in these regions when the polarizers are parallel [see Figs. 1(a) and 1(b), (i) and (v)].

Comparing experimental observations with the theoretical predictions (Fig. 6) for crossed ($\chi = 90°$) and for parallel ($\chi = 0°$) polarizers, the agreement is good over most of the latter profile, the curves decreasing monotonically. Differences arise only at the extreme edge of the profile: the experimental data do not reach zero. The photograph of the image shown in Fig. 1 suggests a sharper boundary than the data indicate. However, the printing process is likely to have contributed to a sharpening of the edge, because it has been shown that the film response and the scanning procedure do not distort the images. Hence the experimental data, determined from the negatives, are more truly representative. It is possible that a degree of forward scatter at the extreme edge of S2 increases the light intensity in this region.

For the crossed polarizers ($\chi = 90°$) there are greater discrepancies between theory and experiment. Both curves peak close to the edge of the structure, but the experimental peak is broader than its theoretical counterpart. It is possible to fit data to theory on the rising part of the curve, but then the experimental curve is lower by more than a factor of 4. Since the theory has accounted for the transmission factors and Lambertian illumination, it is difficult to ascertain the reason for the differences.

The issue of birefringence has not been raised in this paper because neither of the structures has shown any

evidence of measurable birefringence, i.e., in the form of isochromatics (colored fringes in the images between crossed polarizers). For this reason the analysis was made purely in terms of rotation of linear polarization with no consideration given to elliptical or circular polarization.

The study of polarization patterns and how they relate to the refractive properties of the structure in which they are seen has practical application in eye research. The notion that the isogyre patterns seen in the refractive elements of the eye were a sign of birefringence has been challenged recently for both the eye lens[1] and the cornea.[10] The purpose of these studies was not to negate the possibility of some refractoanisotropy in these elements but rather to indicate that the primary reason for the isogyre pattern is not anisotropy but its relationship to the refractive properties (curvature, refractive-index profile) of the structure. Indeed, a qualitative relationship between refractive properties, the isogyres, and the contours of light intensity in the quadrants has been demonstrated.[6] The eye lens is a gradient-index structure, which complicates the direct measurement of the index variations. Nondestructive measurements have relied on ray tracing,[11–14] which necessitated assumptions in the mathematical derivations. A quantitative link with the polarization patterns would provide another means of assessing the refractive index and would aid in confirming or refuting the assumptions inherent in ray-tracing analyses.

A clinically relevant application of this work lies in a study of the cornea. An isogyre pattern similar to the one that is seen when one is looking at the living cornea with a biomicroscope (a standard clinical instrument for viewing the anterior eye), using polarized light, has been produced on the surfaces of curved, reflecting structures subjected to the same viewing conditions.[10] It is likely that the corneal isogyres are also a result of reflection and the subsequent rotation of the vibration direction of the rays depending on the angle of reflection and as such are explained in essentially the same way as for refracted rays. A quantitative method of relating the isogyre pattern to corneal shape would have a useful and inexpensive clinical application. Studies such as the one presented in this paper are needed to provide the necessary background information.

ACKNOWLEDGMENTS

B. K. Pierscionek is supported by the National Health and Medical Research Council of Australia and acknowledges financial support from Essilor International. R. A. Weale's comments and the photographic expertise of John Doyle and Lindsay Howe are gratefully acknowledged.

Correspondence should be addressed to Barbara K. Pierscionek at the address on the title page or by e-mail: b.pierscionek@ee.latrobe.edu.au, or fax: 613-9-471-0524.

REFERENCES

1. B. K. Pierscionek, "Explanation of isogyre formation by the eye lens," Ophthalmol. Physiol. Opt. **13**, 91–94 (1993).
2. W. N. Charman, "Explanation for the observation of isogyres in crystalline lenses viewed between crossed polarizers," Ophthalmol. Physiol. Opt. **13**, 209–211 (1993).
3. B. K. Pierscionek and D. Y. C. Chan, "Mathematical description of isogyre formation in refracting structures," Ophthalmol. Physiol. Opt. **13**, 212–215 (1993).
4. J. Lekner, "Isogyre formation by isotropic refracting bodies," Ophthalmol. Physiol. Opt. **15**, 69–73 (1995).
5. L. Baxter, "On the properties of polarization elements as used in optical instruments. III. Angular aperture functions of a positive dichroic film polarizer," J. Opt. Soc. Am. **46**, 435–443 (1956).
6. B. K. Pierscionek and R. Reytomas, "Light intensity distributions in refracting structures placed between crossed polarizers," Exp. Eye Res. **62**, 573–581 (1996).
7. J. Lekner, "Normal-incidence reflection and transmission by uniaxial crystals and crystal plates," J. Phys. Condens. Matter **4**, 1387–1398 (1992).
8. J. Lekner, "Optical properties of a uniaxial layer," Pure Appl. Opt. **3**, 821–837 (1994).
9. J. Lekner, *Theory of Reflection* (Nijhoff/Kluwer, Dordrecht, The Netherlands, 1987).
10. B. K. Pierscionek and R. A. Weale, "Reflection and the corneal cross," Eye (to be published).
11. M. C. W. Campbell, "Measurement of refractive index in an intact crystalline lens," Vision Res. **24**, 409–415 (1984).
12. D. Axelrod, D. Lerner, and P. J. Sands, "Refractive index within the lens of a goldfish eye determined from the paths of thin laser beams," Vision Res. **28**, 57–65 (1988).
13. B. K. Pierscionek, D. Y. C. Chan, J. P. Ennis, G. Smith, and R. C. Augusteyn, "A non-destructive method of constructing three-dimensional gradient index models for crystalline lenses: I. Theory and experiment," Am. J. Optom. Physiol. Opt. **65**, 481–491 (1988).
14. W. S. Jagger, "The refractive structure and optical properties of the isolated crystalline lens of the cat," Vision Res. **30**, 723–738 (1990).